Applied Surface Science 563 (2021) 150373

Contents lists available at ScienceDirect

Applied Surface Science

journal homepage: www.elsevier.com/locate/apsusc

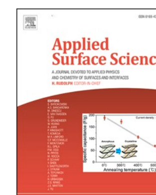

Full Length Article

Atomic layer deposition of tungsten and tungsten-based compounds using WCl_5 and various reactants selected by density functional theory

Minyoung Lee [a,1], Romel Hidayat [b,1], Dip K. Nandi [a], Tae Hyun Kim [a], Yewon Kim [b], Seongyoon Kim [b], Won-Jun Lee [b,*], Soo-Hyun Kim [a,c,*]

[a] School of Materials Science and Engineering, Yeungnam University, 280 Daehak-Ro, Gyeongsan, Gyeongbuk, Republic of Korea
[b] Department of Nanotechnology and Advanced Materials Engineering, Sejong University, Seoul 05006, Republic of Korea
[c] Institute of Materials Technology, Yeungnam University, 280 Daehak-Ro, Gyeongsan, Gyeongbuk 38541, Republic of Korea

ARTICLE INFO

Keywords:
Atomic layer deposition
Tungsten
WCl_5
Density functional theory
Chemisorption energy
XPS

ABSTRACT

Atomic layer deposition (ALD) of metals and metal nitrides consist a major portion of the advanced thin film deposition technology owing to their wide applications in the field of the semiconductor industry. In this regard, the ALD of tungsten (W) is one of the vital processes which is mostly studied using WF_6 precursor. However, the presence of corrosive fluorine in WF_6 restricts its applications due to severe disadvantages like F-contamination and etching of the deposited films and/or the underlying substrate. Therefore, developing F-free W (FFW) precursor to deposit W (and other W-based compounds like WN_x) is of significant importance. The current article investigates several possible routes that can give rise to the successful growth of ALD-W or W-based thin films using WCl_5 as an FFW precursor. Density functional theory (DFT) simulation was carried out to check the feasibility of the reactions between a reactant and tungsten chloride as well as to predict the composition of the deposited film. The exothermic reactions for ALD of W metal were realized with H, diethylamine borane (DEAB), and dimethylamine borane (DMAB), whereas it was endothermic for H_2, triethylaluminum (TEA), trimethylaluminum (TMA), *tert*-butyl hydrazine (TBH), and NH_3. The detailed reaction mechanisms for predicting the growth of tungsten or tungsten compounds were simulated and are helpful to explain the growth of WN_xC_y by TBH and WC_x by TEA. On the other hand, the experimental findings also confirm the W film deposition with H_2 plasma and DEAB, between 200 and 300 °C. However, the best quality as-grown W-films (polycrystalline with a resistivity of ~395 μΩ-cm) were obtained only with H_2 plasma as a reactant, which shows the largest negative reaction energy (ΔE) in DFT calculation. Further, the Cl content of much below 1 atomic% in the as-grown films deposited with H_2 plasma was evident. Additionally, the experimental findings also confirmed the deposition of crystalline-W_2N when NH_3 was used as a reactant.

1. Introduction

Atomic layer deposition (ALD) is one of the most promising technologies related to preparing thin films for microelectronic device fabrication [1,2]. Owing to its self-limiting growth on the surface, ALD possesses several key features, including the capability of depositing highly uniform, pure, ultrathin films with extremely high step coverage in a complicated geometry, which enables this technique one of the favorites in semiconductor device applications [3,4]. Tungsten (W) ALD is one of the most successful case among elemental metal ALD processes. This is because W ALD can be carried out using well-known and the most effective combination of W-containing inorganic precursor, WF_6, and reducing agents, such as silane (SiH_4), disilane (Si_2H_6), and diborane (B_2H_6) [5–8]. Thin films of ALD-W has many applications for the semiconductor device fabrications, including W-plug process, W metal lines such as gate, bit line of DRAM (dynamic random access memory), or gate of 3D NAND Flash due to its relatively low bulk resistivity (~5.6 μΩ·cm for α-W), high melting point, hard, and considerable inert nature [6,9]. With unlimited and continuous device scaling, now it has been even considered as an alternative to the current Cu metal line due to a

* Corresponding authors at: School of Materials Science and Engineering, Yeungnam University, 280 Daehak-Ro, Gyeongsan, Gyeongbuk, Republic of Korea (S.-H. Kim). Department of Nanotechnology and Advanced Materials Engineering, Sejong University, Seoul 05006, Republic of Korea (W.-J. Lee).
E-mail addresses: wjlee@sejong.ac.kr (W.-J. Lee), soohyun@ynu.ac.kr (S.-H. Kim).
[1] These authors contributed equally.

https://doi.org/10.1016/j.apsusc.2021.150373
Received 30 March 2021; Received in revised form 20 May 2021; Accepted 11 June 2021
Available online 15 June 2021
0169-4332/© 2021 Elsevier B.V. All rights reserved.

shorter electron mean free path (EMFP, ~19 nm) than that of Cu (~39 nm) though Cu has lower bulk resistivity (~1.7μΩ·cm) [10]. Here, W thin film has been typically formed in two steps; the first step is the very thin W nucleation layer (2 ~ 3 nm) deposited by ALD on typical glue/barrier layer, TiN film, and the second is the thick bulk W deposition mostly accomplished by a CVD process or H_2 reduction of WF_6 [11]. Extensive studies on ALD-W using WF_6 have been reported since Klaus *et al.* firstly reported the formation of metallic W film with the resistivity of 122 μΩ·cm by a sequential supply of WF_6 and Si_2H_6 at the temperature of lower than 325 °C [7]. However, the use of F-containing inorganic precursor (WF_6) has several potential problems of incorporating corrosive F impurities, resulting in the etching of underlying substrates, degradation of adhesion between layers, and defect formation due to an unwanted reaction with the underlying materials. It has also been reported that F could diffuse into adjacent dielectric layers where it can create yield-limiting defects for preparing the W gate of 3D NAND devices. As a thin TiN layer is inevitable to provide an adhesion layer for W thin film consist of ALD-W nucleation and CVD-W bulk film and to block F penetration, it narrows line or plug opening width with continuous device scaling, resulting in an increase in their resistance and even failure of the plug filling. The deposition of a thin W nucleation layer using an F-free W (FFW) precursor is an ideal solution because it can reduce the thickness of the TiN film or eliminate it. By substituting the conventional TiN liner with W liner, which was prepared by FFW-based technology, the line resistance of PCRAM (phase-change random access memory) contact plugs has been decreased by about 20% [12]. However, the very few reports on W ALD using F-free W precursors are still available, and the details for the FFW ALD process have not been fully reported. One recent report only showed the process details, which is the reaction of WCl_6 as a potential FFW-precursor and trimethylaluminum ($AlMe_3$, TMA) as a reactant between 250 and 375 °C but the deposited film contained a significant amount of C with the high resistivity of 1500 μΩ·cm at 375 °C [13]. Studies of the ALD of W-based films using FFW precursors have been focused mainly on preparing tungsten nitride film. Several attempts have been taken to prepare ALD-WN_x films using F-free metalorganic (MO) precursors such as bis(*tert*-butylimido)bis(dimethylamido) tungsten(VI) [$(^tBuN)_2(Me_2N)_2W$], hexakis(dimethylamido) ditungsten [$W_2(NMe_2)_6$], and tungsten hexacarbonyl [$W(CO)_6$] at temperatures ranging from 150 to 400 °C [14–16]. Moreover, the ALD WSiN process was also reported using FFW precursor bis(*tert*-butylimido)bis(bis(trimethylsilylamido)) tungsten(VI) [$W(N^tBu)_2\{N(SiMe_3)_2\}_2$] and H_2 plasma at 300 °C [17]. Recently, the controlled preparation of WN_x and WC_x thin films via an ALD was carried out using a fluorine- and nitrogen-free W metalorganic precursor of tungsten [tris(3-hexyne) carbonyl, $W(CO)(CH_3CH_2C{\equiv}CCH_2CH_3)_3$] and NH_3 or $N_2 + H_2$ mixture plasma as the reactant at a deposition temperature of 250 °C [18,19].

The ALD of metal requires the reactive reducing agent to remove the ligand of the metal precursor. For the ALD of Cu, different reducing agents were tested for depositing pure copper films, and H_2 [20], H_2 plasma [21], diethylzinc [22], and *tert*-butyl hydrazine [23] showed promising results. H_2 was also used for the ALD of cobalt, iron, and nickel [24]. An aluminum hydride compound was used for the ALD of Al [25]. These results show that the choice of reducing agent is the most critical element for success in the ALD of metallic films. Density functional theory (DFT) calculation was used to expect the surface chemistry during the ALD of copper [26,27]. The DFT method was also used to investigate the reaction mechanism of formate and hydrazine as reducing agents for three-step ALD of copper using Cu(OCH-MeCH$_2$–NMe$_2$)$_2$ precursor [28]. Recently, we reported the DFT study on atomic hydrogen, H_2, B_2H_6, and SiH_4 as the reducing agent for the ALD of tungsten [29]. Therefore, the DFT simulation explains the ALD reaction mechanism and helps to select the appropriate reducing agent [30]. However, the results of the DFT study were not verified by ALD experiments. In addition, only reducing agents used in the CVD or ALD process using WF_6 were considered.

In this study, we report ALD processes using tungsten pentachloride (WCl_5) as an FFW precursor and various reactants. WCl_5 is fluorine-free and produces HCl as the reaction byproduct, which is less critical to dielectrics compared with HF produced by WF_6. We selected WCl_5 rather than WCl_6 because WCl_5 has a higher vapor pressure than WCl_6, which facilitates better delivery of the precursor into the chamber and makes the process more repeatable. We performed the density functional theory (DFT) calculations to select the most feasible reducing agents for WCl_5. A variety of molecules were selected, which have not been considered in the previous study [29], and their chemisorption reactions were simulated. Based on the DFT results, we performed the deposition experiment using WCl_5 and selected reducing agents. The elemental compositions, crystallographic nature, and resistivity of the as-grown films were studied using several *ex-situ* characterization tools such as XPS, XRD, and four-probe measurements.

2. Material and methods

2.1. Computational methods

The calculations were performed using Materials Studio 7.0 using the DMol^3 Package (Accelrys, USA) [31]. The exchange correction functional of generalized gradient approximation (GGA) with the Perdew-Burke-Ernzerhof (PBE) scheme correction [32] and the double numerical polarization (DNP) 4.4 basis set [33] were applied. Since tungsten has many electrons, an effective core potential treatment was also applied [34,35], which replaces the core electron with a single potential and introduces some relativistic corrections into the core. The unrestricted spin option was applied to perform the calculation with different orbitals for different spins [36]. The convergence tolerance of total energy difference, atomic force, and orbital occupancy smearing used in the geometry optimization were 10^{-6} Ha, 2×10^{-4} Ha/Å, and 9×10^{-4} Ha (1 Ha = 27.2114 eV), which were the same as our previous works [37–39].

We considered a various type of molecules as the reducing agents: atomic hydrogen (H), hydrogen (H_2), silane (SiH_4), disilane (Si_2H_6), diborane (B_2H_6), dimethylamine borane [DMAB, $(CH_3)_2NHBH_3$], diethylamine borane [DEAB, $(C_2H_5)_2NHBH_3$], diisopropylamine borane [DIPAB, $(i\text{-}C_3H_7)_2NHBH_3$], germane ($GeH_4$), digermane ($Ge_2H_6$), ammonia ($NH_3$), hydrazine ($N_2H_4$), *tert*-butyl hydrazine [TBH, $(CH_3)_3CNHNH_2$], acetonitrile (MeCN, CH_3CN), trimethylaluminum [TMA, $Al(CH_3)_3$], and triethylaluminum [TEA, $Al(C_2H_5)_3$]. H_2, SiH_4, Si_2H_6, B_2H_6, GeH_4, and Ge_2H_6 were selected because they were reported as the reducing agent for ALD or CVD of W using WF_6 [5–9,11,39–43]. NH_3, N_2H_4, and TBH were selected because they were tested as the reducing agent for ALD of Cu [13,44,45]. Alkyl aluminum compounds and alkylamine boranes were also considered because of their strong reducing powers [46,47].

The reactivities of reducing agents were evaluated by comparing reaction energies to remove the Cl atom from the Cl-passivated tungsten cluster, W_4Cl_{12}, which is an adequate cluster model reported in the previous work [29]. Other reaction pathways were also considered to expect the mechanism for the formation of tungsten compounds. The unbound reactant (UR), reactant (R), and product (P) states were defined. The UR state is the system after geometry optimization of the reducing agent molecule located at about 9 Å from the cluster. The R state is the physisorption obtained by placing the reducing agent molecule approximately 4 Å away from the cluster and then performing geometric optimization. The P state was obtained by assuming possible reaction pathways for removing one chlorine atom from the cluster. Reaction energies were evaluated to determine the feasible routes from considered reaction pathways for the selected reducing agent. The activation energies of the exothermic reaction pathways were calculated to expect the reaction rate. The adsorption energy (E_{Ads}), reaction energy (ΔE), and activation energy (E_A) were calculated following Eqs. (1)–(3):

$$E_{Ads} = E_R - E_{UR} \quad (1)$$

$$\Delta E = E_P - E_R \quad (2)$$

$$E_A = E_{TS} - E_R \quad (3)$$

where the E_{UR}, E_R, and E_P are the total system energy of the UR, R, and P states, respectively. E_{TS} is the total energy of the transition state between R and P states obtained by the complete linear-quadratic synchronous transit (LST-QST) method [48].

2.2. ALD processes

ALD of W-films were performed in a shower-head type ALD reactor (Lucida-M100, NCD Technology) also equipped with a radio-frequency (RF) power source to generate the plasma of the several reactant gases. The reactor wall was heated to a certain higher temperature as calibrated beforehand to achieve the desired deposition temperature of the substrate. While the deposition temperature was varied from 200 to 300 °C, the reactor wall temperature was set as 220–330 °C. For a sufficient vapor pressure of WCl_5, the precursor bubbler was heated at 110 °C while the precursor delivery lines were kept constant at 120 °C to avoid any unintentional condensations of WCl_5. High-purity Ar (200 sccm) was used as a purging gas in between two successive pulses of the precursor and the reactant. The base pressure of the reactor chamber was achieved as 8 mTorr while the working pressure during the reaction was set as ~ 400 mTorr with the help of Ar purging. In addition, 50 sccm Ar was also used as a carrier gas for the smooth delivery of the WCl_5 precursor. While the reactants like TMA, TEA, DEAB, DMAB, and TBH were kept at a constant temperature, all the gaseous reactants (like NH_3 and H_2) were fed to the reactor line from room temperature with the flow rate of 50 sccm. Co-reactants of TMA, TEA, DEAB, DMAB, and TBH that are liquid at the supplying temperature and contained at the bubbler are mixed with the inert carrier gas (Ar: 50 sccm) and supplied into the chamber The temperature of each co-reactant during the providing was kept at 60, 25, 55, 10 °C for DEAB, TBH, TEA, and TMA, respectively. Si substrates (with 100 nm SiO_2 layer on top) were used to grow the films and for further characterizations of them. In general, one ALD cycle consisted of 10 s pulsing of WCl_5-10 s purging of Ar-10 s pulsing of reactant-10 s pulsing of Ar, unless stated otherwise. A repetition of the above sequence results in the growth of ALD-W thin films. A fixed number of 1000 ALD cycles were used to grow the films using different reducing agents. In case of H_2 plasma, 100 W plasma power was applied to generate the H radicals.

2.3. Analytical methods

Grazing incidence angle ($\omega = 3°$) X-ray diffraction (GIA-XRD, PANalytical X'-pert PRO MRD with Cu K_α radiation at 1.54 kW) was carried out of the as-grown ALD films to find out the crystallinity with their corresponding phases. X-ray reflectivity (XRR) and/or cross-sectional view scanning electron microscopy (SEM, Hitachi S-4800) analysis were performed to determine the thickness, density, and uniformity of the films. The presence of the W with different oxidation states and other elements (N in W_2N and the impurities like Cl) and their respective atomic percentages were further estimated by X-ray photoelectron spectroscopy (XPS, ESCALAB 250 XPS Spectrometer with Al K_α source in Korea Basic Science Institute Busan, Korea). Finally, the sheet resistance of the as-grown films deposited with different reactants was measured using a four-probe and compared to sort out the best reactant in view of the electrical properties of the ALD-W.

3. Results and discussion

3.1. DFT calculation on the reaction of WCl_5 and various reactants during ALD

We used the chlorine-passivated tungsten cluster, W_4Cl_{12}, to model the surface after sufficient tungsten chloride exposure, as shown in Fig. S1. The cluster model can minimize the calculation time of the DFT study compared with a periodic slab model, especially in the case of heavy metals with a large number of electrons [34]. To minimize the accuracy issue of the cluster model [49,50], we fully passivated the tungsten cluster with chlorine atoms. The optimization of the numbers of tungsten and chlorine atoms was described in the previous study [29]. The reaction of reducing agent candidates with W_4Cl_{12} was simulated to expect the reducing power of the candidates to produce W metal. The reaction assumed is described in Eqs. (4) and (5):

$$-W{-}Cl^* + R{-}H \rightarrow -W{-}H^* + R{-}Cl \quad (4)$$

$$-W{-}Cl^* + H \rightarrow -W^* + HCl \quad (5)$$

where asterisk (*) denotes the surface group. R–H is the reducing agent molecule, and R–Cl is a chlorinated byproduct molecule.

Fig. 1 shows the reaction energies of different reducing agent candidates for the reactions in Eqs. (4) and (5). The reaction energies were calculated by Eq. (2). The exothermic reactions were expected for H, B_2H_6, DEAB, DMAB, SiH_4, Si_2H_6, GeH_4, and Ge_2H_6, suggesting that those candidates are promising. The endothermic reactions were obtained for H_2, TEA, TMA, MeCN, TBH, N_2H_4, and NH_3, which would be expected to be the less suitable reducing agents to make W metal using tungsten chloride precursor. We already reported the reactions of an H_2 molecule and atomic H in the previous work [29]. The results showed that the reaction of Eq. (4) was unfavorable for H_2, but the reaction producing two HCl molecules and bare tungsten surface, –W*, was marginally favorable with the high activation energy of +2.32 eV. H representing the H_2 plasma species showed the exothermic reaction with a low activation energy of +0.04 eV. Therefore, it was expected that H_2 plasma would be an excellent reducing agent for tungsten chlorides in view of producing W metal, and the deposition with H_2 might be possible at high temperatures. In this study, the more detailed reactions of the selected reactants on the cluster were studied to elucidate the reaction pathways and corresponding formation of various W-containing films.

3.1.1. DEAB and DMAB as a reactant

Fig. 2 shows the schematic and energy diagrams of eight reaction pathways between DEAB and W_4Cl_{12}. Among them, pathways I and IV were expected as the exothermic processes. The reaction energy of pathway I was −0.31 eV with an activation energy of +0.28 eV, whereas the reaction energy of pathway IV was −0.80 eV with an activation

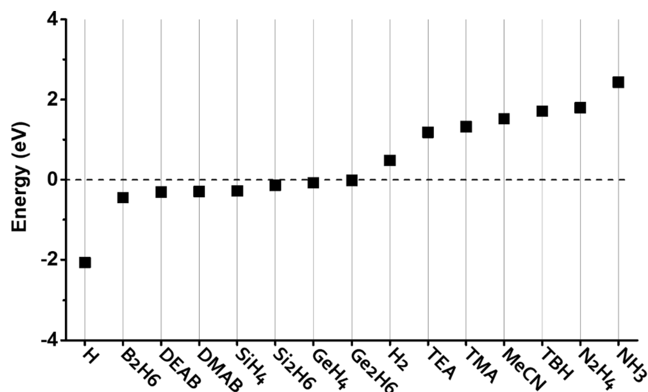

Fig. 1. The reaction energies of reducing agent candidates with W_4Cl_{12} for the reaction in Eqs. (4) and (5). The reaction energies were calculated by Eq. (2).

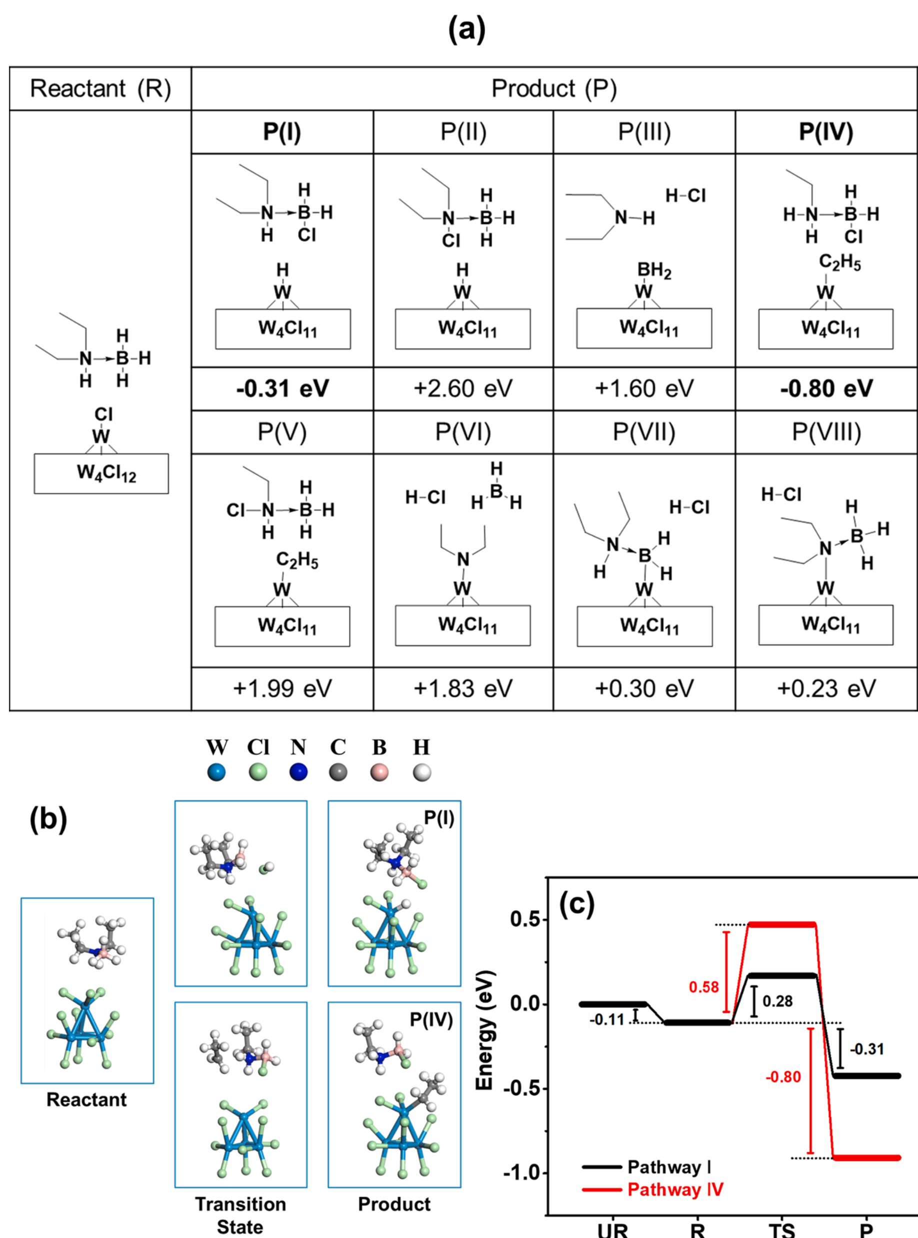

Fig. 2. (a) The schematic of the reactant and product states for eight reaction pathways of DEAB with W_4Cl_{12}, (b) atomistic configurations, and (c) energy diagrams for the reaction pathways I and IV (UR, unbound reactant state; R, reactant state; TS, transition state; P, product).

energy of +0.58 eV. Pathway I is the exchange of H from DEAB with chlorine on the cluster, resulting in –W–H* and $NH(C_2H_5)_2BH_2Cl$ byproduct. The growth of metallic tungsten is expected because –W–H* ensures no impurity. Pathway IV is the chlorine abstraction by boron of DEAB and the C_2H_5 migration to the tungsten cluster, forming –W–C_2H_5* and $NH_2(C_2H_5)BH_2Cl$ byproduct. The formation of –W–C_2H_5* would lead to the tungsten carbide deposition or the carbon contamination in the tungsten film if the next half-reaction of WCl_5 with –W–C_2H_5* forms –W–C_2H_{5-n}–WCl_{5-n}* and HCl molecules. Both pathways would be fast enough at ALD process temperatures due to their low activation energies. Therefore, the DFT calculation result expects that the use of DEAB would produce the tungsten film with carbon contaminations.

Both pathways IV and V form –W–C_2H_5*, but pathway IV is an exothermic reaction, whereas pathway V is endothermic. It is because the byproduct molecule is more stable for pathway IV. The byproduct molecule is NH_2Et-BH_2Cl for pathway IV and NHCl-EtBH_3 for pathway V. We calculated the bond dissociation energies by DFT. The dissociation energies of N–H (3.96 eV) and B–Cl (5.26 eV) bonds in the NH_2Et-BH_2Cl molecule are higher than those of the N–Cl (1.94 eV) and B–H (4.56 eV) bonds in the NHClEt-BH_3 molecule.

Fig. S2 shows the schematic and energy diagrams of eight reaction pathways between DMAB and W_4Cl_{12}. Similar to the DEAB case, pathways I and IV were expected as the exothermic processes. Pathway I is the exchange of H from DMAB with chlorine on the cluster, resulting in –W–H* and $NH(CH_3)_2BH_2Cl$ byproduct. Pathway IV is the chlorine abstraction by boron of DMAB and the CH_3 migration to tungsten cluster, forming –W–CH_3* and $NH_2(CH_3)BH_2Cl$ byproduct. The reaction energy of pathway I was −0.30 eV with an activation energy of +0.61 eV, whereas the reaction energy of pathway IV was −0.74 eV with an activation energy of +0.83 eV. The formation of –W–CH_3* would also lead to the tungsten carbide deposition or the carbon contamination in the tungsten film. Therefore, similar to DEAB, the deposition of tungsten film with carbon contaminations was expected. Meanwhile, DMAB would be less reactive than DEAB due to the higher activation energies.

3.1.2. TEA and TMA as a reactant

The reaction of TMA with the W_4Cl_{12} cluster was already reported in previous work [29]. The only exothermic reaction was the exchange of CH_3 of TMA with chlorine on the cluster, forming –W–CH_3* and Al$(CH_3)_2$Cl byproduct. Tungsten carbide film will grow if –W–CH_3* reacts with WCl_x precursors forming –W–C–W–Cl* and HCl byproducts. In the present work, we compared TEA with TMA. Fig. 3 shows the schematic and energy diagrams of four reaction pathways between TEA and W_4Cl_{12}. The only exothermic process was pathway II, which is the exchange of C_2H_5 of TEA with chlorine on the cluster, forming –W–C_2H_5* and Al$(C_2H_5)_2$Cl byproduct. The reaction energy was −0.93 eV with an activation energy of +0.34 eV. Therefore, in the same way as TMA, TEA was expected to act as a carbon source to grow tungsten carbide films if –W–C_2H_5* reacts with tungsten chlorides to form –W–C_2H_{5-n}–WCl_{5-n}* and HCl byproducts. It is noted that TEA would be more reactive than TMA due to its higher reaction energy and lower activation energy.

3.1.3. TBH and NH_3 as a reactant

Fig. 4 shows the schematic and energy diagrams of eight reaction pathways between TBH and W_4Cl_{12}. Pathways V and VIII were expected as the exothermic processes. Pathway V is the exchange of $NHNH_2$ of TBH with chlorine on the cluster, producing –W–$NHNH_2$* and ^{t}BuCl byproduct. Pathway VIII is the exchange NHNH^{t}Bu of TBH with chlorine on the cluster, forming –W–NHNH^{t}Bu* and HCl byproduct. The reaction energy of pathway V was −0.29 eV with an activation energy of +1.50 eV, whereas the reaction energy of pathway VIII was −0.32 eV with an activation energy of +0.42 eV. Pathway VIII would dominate the deposition reaction because of lower activation energy than pathway V. Therefore, tungsten carbonitride film would grow if –W–NHNH^{t}Bu* reacts with tungsten chlorides. The possible subsequent half-reaction pathways are as follows:

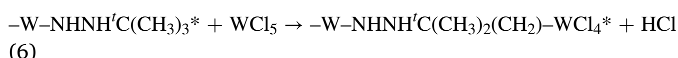

$$-W-NHNH^tC(CH_3)_3^* + WCl_5 \rightarrow -W-NHNH^tC(CH_3)_2(CH_2)-WCl_4^* + HCl \quad (6)$$

$$-W-NHNH^tC(CH_3)_3^* + WCl_5 \rightarrow -W-NHNH^tC(CH_3)_2-WCl_4^* + CH_3Cl \quad (7)$$

$$-W-NHNH^tC(CH_3)_3^* + WCl_5 \rightarrow -W-NHNH-WCl_4^* + (CH_3)_3CCl \quad (8)$$

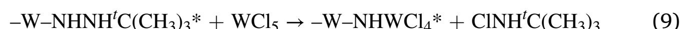

$$-W-NHNH^tC(CH_3)_3^* + WCl_5 \rightarrow -W-NHWCl_4^* + ClNH^tC(CH_3)_3 \quad (9)$$

Fig. 5 shows the schematic and energy diagrams of three reaction pathways between NH_3 and W_4Cl_{12}. The only exothermic process was pathway II, where NH_2 of NH_3 is exchanged with chlorine of the cluster, forming –W–NH_2* and HCl. The reaction was marginally exothermic, with the reaction energy of −0.004 eV and the activation energy of +1.51 eV. Tungsten nitride films would grow using the NH_3 if –W–NH_2* reacts with tungsten chlorides to form –W–$NH_{2\text{-}n}$–$WCl_{5\text{-}n}$*.

3.2. Atomic layer deposition using WCl_5 and selected reducing agents

Experiments on ALD-W or W-based films were carried out in detail to verify the theoretical evidence obtained by DFT calculations. Prior to performing the sequential dosing of WCl_5 with several individual reactants, the possibility of thermal decomposition of the metal precursor was confirmed in the complete deposition temperature range (200–300 °C). The absence of any thermal decomposition of the W-precursor resulted in no sign of any film deposition on the substrates after continuous dosing of the only WCl_5 even at 300 °C. Henceforth, the ALD of W-based films was investigated using eight different reducing agents that include molecular H_2, H_2 plasma (which provides highly reactive H radical), TMA, TEA, DEAB, DMAB, TBH, and NH_3 molecules. A few reactants (B_2H_6, SiH_4, Si_2H_6, GeH_4, and Ge_2H_6) to show a thermodynamically favorable reaction with WCl_5, in view of producing W metal from DFT calculations (Fig. 1) could not be tested experimentally due to the present limitations. On the other hand, the reactions between WCl_5 with TBH or NH_3 molecules were executed because of the possibility of a tungsten nitride (WN_x) or tungsten carbonitride film (WN_xC_y) film's growth as observed for WF_6, which also have many applications for semiconductor device fabrication including diffusion barriers, capacitor or gate electrode [51–53]. Finally, molecular H_2 was also tested as a reactant to verify one of the negative results obtained in the DFT calculation and establish the distinct difference between H_2 molecules and H_2 plasma towards reducing WCl_5 to give rise to the deposition of W-metal.

The depositions with each reactant were carried out at three different

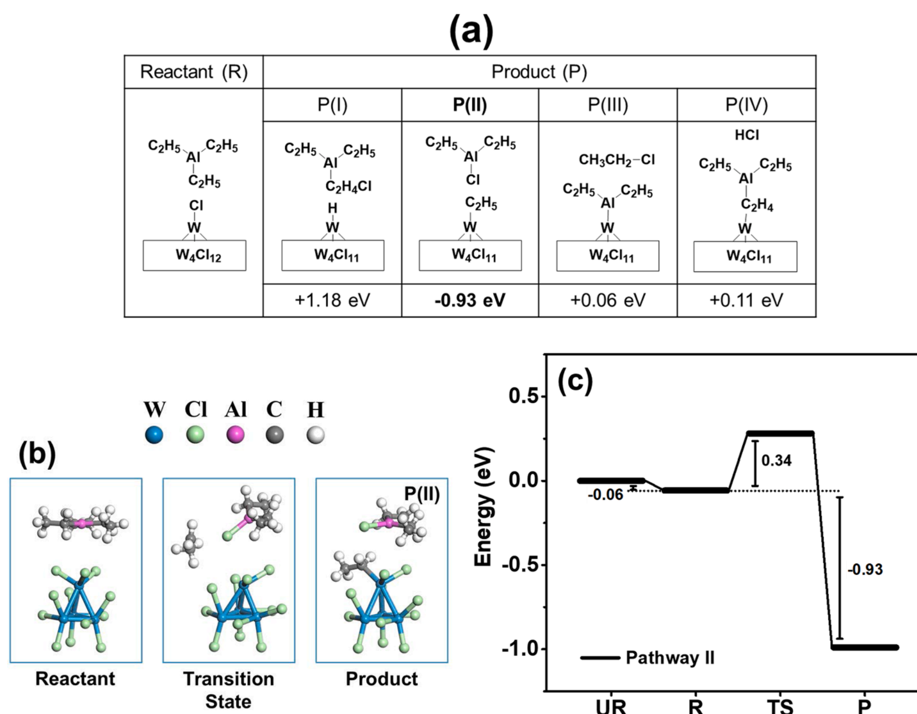

Fig. 3. (a) The schematic of the reactant and product states for four reaction pathways of TEA with W_4Cl_{12}, (b) atomistic configurations, and (c) energy diagram for the reaction pathway II (UR, unbound reactant state; R, reactant state; TS, transition state; P, product).

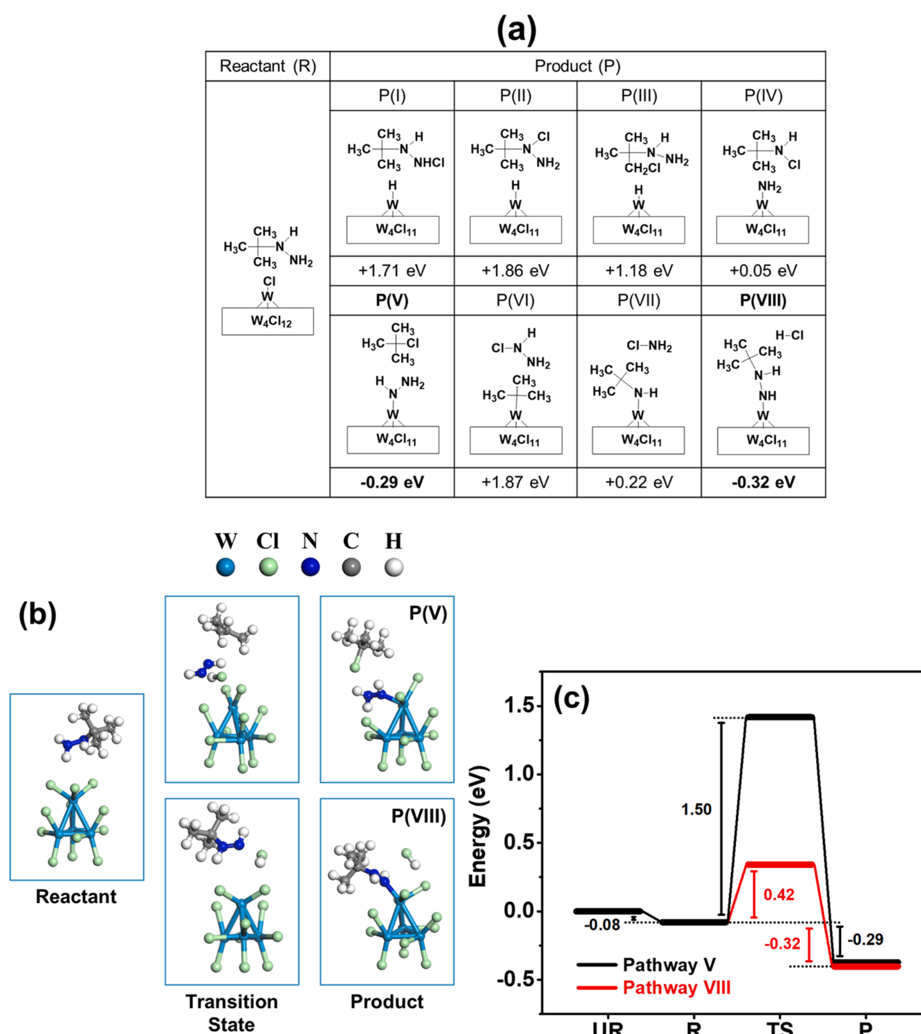

Fig. 4. (a) The schematic of the reactant and product states for eight reaction pathways of TBH with W_4Cl_{12}, (b) atomistic configurations, and (c) energy diagrams for the reaction pathways V and VIII (UR, unbound reactant state; R, reactant state; TS, transition state; P, product).

temperatures (200, 250, and 300 °C). The reaction sequence was set as 10 s WCl_5 pulsing-10 s Ar purging (Ar)-10 s reactant pulsing-10 s Ar purging during every deposition carried out in this work. The repetition of the above sequence ensures the ALD, probably under self-limiting condition owing to the large enough pulsing time for both precursor and reactant. Table 1 depicts the overall outputs as successful depositions (by the symbol "O") and failure of any kind of film's formation (by a symbol "X") at these three deposition temperatures corresponding to each reactant. Successful deposition of the films could be observed only with H_2 plasma, DEAB, TEA (only at 300 °C), TBH, and NH_3 against WCl_5 via ALD. On the other hand, we could not find any film to be deposited while TEA (200 and 250 °C), TMA, and DMAB were used as respective reactants. In addition, molecular H_2 also failed to result in any deposition, which is in good agreement with the DFT calculations except DMAB that indicated a possibility of depositing W films with some C contamination similar to DEAB (Fig. 2 and Fig. S2). While TEA and TMA both showed an endothermic reaction in DFT calculation towards W metal deposition (Fig. 1), WC_x based films might be deposited with WCl_5 with a more favorable reaction with TEA compared to TMA considering the reaction pathways (Fig. 3). Therefore, the experimental findings supported well, to some extent, the DFT predictions. Here, one should notice that thermal ALD of WC_x was prepared with WCl_6 and TMA [13]. Therefore, a higher deposition temperature above 300 °C might lead to form WC_x film using WCl_5, which is however not the primary goal of this work. On the other hand, the use of NH_3 and TBH (more reactive than NH_3) showed the possible deposition of tungsten nitride and tungsten carbonitride but not for W metal, which is complemented through the further characterizations of the experimentally deposited films.

The presence of the films and their corresponding growth per cycle (GPC) values were estimated by cross-sectional view-SEM (XSEM) imaging. Table S1 shows the GPC for each film grown at 300 °C using 1000 ALD cycles. While the H_2 plasma and NH_3 revealed a GPC of ~0.27 and 0.37 Å, respectively, a much higher GPC of ~0.8 Å were evident for both TBH and DEAB. However, TEA also showed a relatively lower GPC of ~0.2 Å. The higher GPC values obtained for the TBH and DEAB could be realized from a formation of a not well-defined films (possibly a ternary film like oxynitride or oxycarbide) that might have significant impurities and unreacted precursors. On the other hand, TEA reactivity seems to be the lowest among all reducing agents as it does not give rise to any deposition at a lower deposition temperature below 300 °C. In addition, we have estimated the incubation period for the films grown with H_2 plasma and NH_3 which enabled to deposit well-defined crystalline W and W_2N films, respectively, as discussed later. The incubation period (on SiO_2/Si substrate) was calculated as ~ 65 and 78 ALD cycles for W and W_2N films, respectively. Fig. S3 shows the XSEM images of the films grown with different reducing agents using 1000 ALD cycles. The XSEM images clearly confirm smooth, uniform, continuous pin-hole free depositions of the films with different thicknesses. Thus, these preliminary experiments indicate the successful film formation with different reactants with WCl_5 and further detail study with each of them can

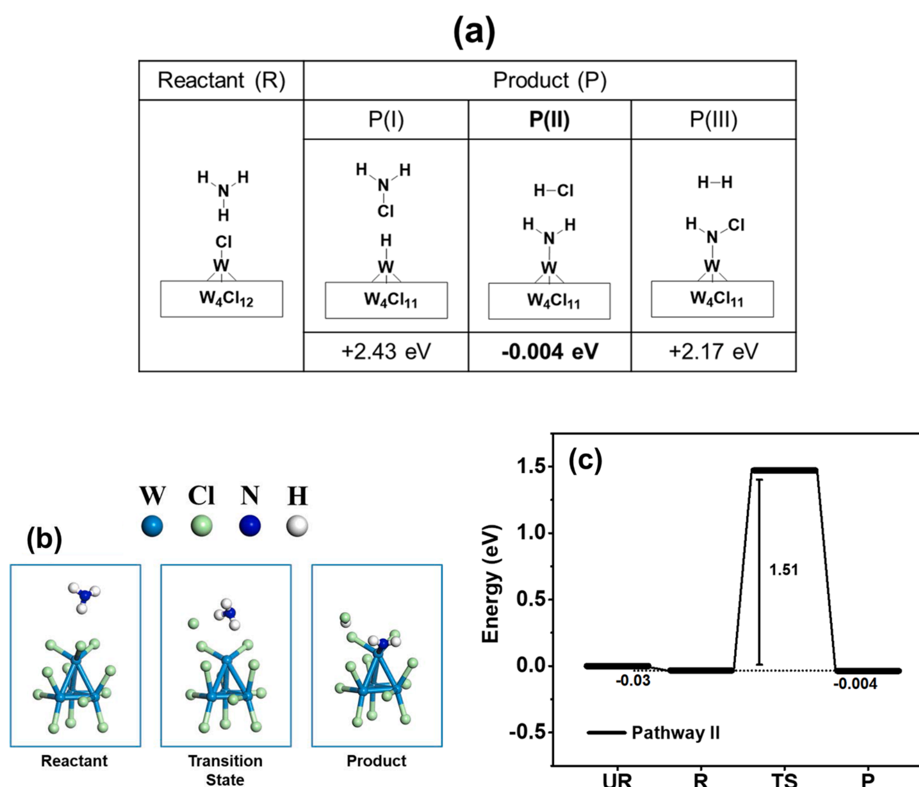

Fig. 5. (a) The schematic of the reactant and product states for three reaction pathways of NH_3 with W_4Cl_{12}, (b) atomistic configurations, and (c) energy diagram for the reaction pathway II (UR, unbound reactant state; R, reactant state; TS, transition state; P, product).

Table 1
Confirmation of the deposition of films while WCl_5 reacting with several reactants at three different temperatures.

Reactant/Dep. Temp.	200 ℃	250 ℃	300 ℃
Thermal decomposition (5 min)	X	X	X
H_2	X	X	X
H_2 Plasma (100 W)	O	O	O
Diethylamine Borane (DEAB)	O	O	O
Dimethylamine Borane (DMAB)	X	X	X
Triethyl Aluminum (TEA)	X	X	O
Trimethyl Aluminum (TMA)	X	X	X
tert-Butyl hydrazine (TBH)	O	O	O
NH_3	O	O	O

establish a separate process with more specific outcomes.

Fig. 6 shows the GIAXRD patterns of the thin films grown individually with H_2-plasma, DEAB, TEA, TBH, and NH_3 reactants on Si/SiO_2 substrates at 300 °C. Several peaks corresponding to metallic-W were identified for the film deposited with WCl_5 and H_2 plasma. It is well-known that the metallic-W mainly exists in two phases, namely β-W (A-15 structure) and α-W (body-centered cubic (bcc) or A-2 structure), while the former is metastable and the latter is the most stable phase [54]. The properties, such as resistivity or hardness, vary significantly for these two phases, and the phase formation depends on several parameters like deposition temperature, pressure, power, post-annealing, and substrates [55]. Detailed analyses of these XRD peaks revealed that the film consists of both β- and α-W phases. While the peak at 2θ values of 39.9° could be assigned to β(210)/α(110), most of the other signature peaks are from β-W corresponding to (200), (211), and (222) planes at 2θ values of ca. 37.4, 43.5, and 63.4°, respectively. On the other hand, the XRD peak at ~ 73.2° could be ascribed to the (211) planes of the α-W phase. Thus, it could be concluded that the successful ALD of W thin films using WCl_5 and H_2 plasma resulted in as-grown films consisting more of β-phase. It was reported several times earlier, including ALD of W using WF_6 and SiH_4, that the W thin films transform from amorphous (or poor crystalline) phase to crystalline phase and similarly from meta-stable β to body-centered cubic (bcc) α phase with increasing deposition temperature [5]. In addition, it was also observed that the phase transition from β/(β + α) to α also got influenced by the thickness of the film for a particular temperature, and this critical thickness varies for individual studies, generally lying between ~ 20 to 75 nm [56,57]. The residual stress developed in the thicker film was identified as the probable cause for such phase transformation [56]. Therefore, achieving the films with a pure α-W phase using the current ALD recipe would be possible. We believe that a pure α-W will be achieved by increasing the thickness of the film or by performing a post-annealing in an inert (Ar) or reducing (H_2) environment. Moreover, such thickness increment or post-annealing should also reduce the resistivity of the films compared to the as-grown films owing to its transformation into pure α phase. Unfortunately, no XRD peak was found when DEAB was used as a reactant, and therefore, it should be assumed as an amorphous film. Similarly, the amorphous film was also evident with TEA as a reactant. However, TBH might give rise to poor nano-crystallinity in the film, as reflected by a broad hump in the XRD. Though the major peaks of metal-W lie within this broad 2θ range, the presence of WN_x (β-W_2N) and WC_{1-x} (α-W_2C) phases within this similar region are also simultaneously possible [18]. Above all, such a broad peak in the XRD was also observed during the formation of tungsten carbonitride (WN_xC_y) which might be formed as a solid solution of WN_x and WC_{1-x} [58]. Two crystal planes at 2θ of ca. 36.7 and 43.4° corresponding to (111) and (43.2) of β-WN_xC_y could be assigned within this very broad peak observed in the XRD [58]. While the presence of both N and C in the TBH as a reactant has the potential to result in such a ternary phase, the DFT calculation also predicted the formation of carbonitride phase with a relatively lower activation barrier compared to depositing metal W. The formation of ternary compound might prevent the formation of the well-developed crystalline film. The primary target of this work is to confirm the potential of TBH to reduce WCl_5 into W

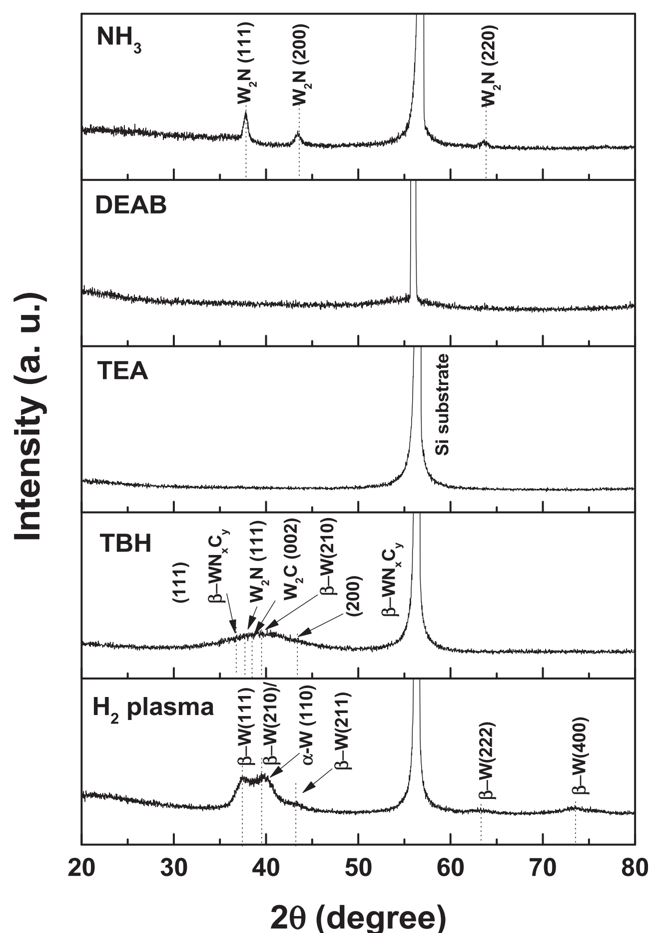

Fig. 6. XRD spectra of the ALD-grown films deposited using WCl_5 with H_2 plasma, TBH, TEA, DEAB, and NH_3, respectively, on Si substrates.

during ALD. Therefore, it could be concluded that TBH alone could not help depositing W films, as also supported by the theoretical calculations. Nevertheless, the existence of the films, which should be close to amorphous, on the substrate could be confirmed from bare eyes and was further confirmed by XPS, as discussed later. On the other hand, the XRD pattern of the film deposited using WCl_5 and NH_3 showed the signature peaks corresponding to tungsten nitrides but not the W metal. Three distinguished peaks at 2θ of ~ 37.7, 43.6, and 63.7° could be assigned to (111), (200), and (220) cubic-W_2N. Thus, the DFT calculations perfectly agree with the experimental evidence of the formation of tungsten nitride in place of metallic tungsten. Earlier, ALD was carried out using WF_6 and NH_3 at a relatively higher temperature of above 300 °C (within 600–800 K ALD window) [52]. It was also reported that the deposition temperature for WN_x formation could be brought down with improved film properties (like resistivity) when diborane (B_2H_6) was introduced as an additional reducing agent to NH_3 [59]. The deposition temperature was also reduced to 200–400 °C using NH_3 pulse-plasma as an additional reactant [60]. However, both of these studies could not resolve the problem of HF as an extremely corrosive byproduct or the unwanted F incorporation in the deposited film. On the other hand, F-free W precursor either leads to an amorphous film [for W $(CO)_6$] or needs NH_3 plasma [for $W(CO)(CH_3CH_2C{\equiv}CCH_2CH_3)_3$] to achieve a crystalline film [16,19]. Therefore, the current study revealed an alternative recipe using FFW-precursor for depositing crystalline ALD-W_2N in a considerably low-temperature window of 200–300 °C.

The as-grown films deposited with different reactants at 300 °C were further characterized with XPS in detail. To avoid the surface contaminations, the films were sputtered using Ar plasma for 30 s, and the spectra were taken. The W thin films deposited WCl_5 and H_2 plasma show the characteristic doublet peaks of W 4f orbital electrons along with a small hump-like peak for W $5p_{3/2}$ at higher binding energy (BE), which is also a common observation along with W 4f spectra as shown in Fig. 7a. The high-resolution XP spectra of W $4f_{7/2}$ and $4f_{5/2}$ for this film are found at BEs (~31.7 and 33.8 eV, respectively) coming from the W (0) of metal-W. The standard database of XPS confirms the BE of W $4f_{7/2}$ orbital electron to lies at 31.3–31.6 eV, which almost matches with the observed value for the films deposited under this current study. The 2.1 eV difference in the BEs between the doublet of W 4f electrons is also in good agreement with the standard value (~2.17 eV). However, further confirmation of the metallic W is justified by its considerably low resistivity, as discussed later in this article. Another most important information reflected from the XPS analyses is about the absence of Cl (Fig. 7b), as we did not find any detectable peak corresponding to Cl 2p orbital electron at its respective BE region. Therefore, it could be confirmed that the current ALD recipe with WCl_5 and H_2 plasma resulted in the W-films with negligibly low Cl impurities and thus overcome the earlier drawback of the deposition process with WF_6, leaving considerable F in the film.

Similar W 4f (~32.2 eV for $4f_{7/2}$) spectra for the ALD films deposited with TBH reactant are shown in Fig. 8a, where the BE values for W orbital electrons are higher compared to W-metal (W^0) and lower compared to WO_3 (35.7 eV$4f_{7/2}$). On the other hand, the W 4f peak position of a solid solution of WC_{1-x} and WN_x could not be distinguished due to their slight separation of 0.2 eV in BE values. In fact, the BE values of W $4f_{7/2}$ and $4f_{5/2}$ at 32.2 and 34.3 eV, respectively, could be ascribed to the W in WN_xC_y [60]. In addition, a broad and not well-defined peak for N1s was identified, as shown in Fig. 8b. This peak is also observed in N 1s owing to the W-N_x (~397.6 eV) and CN_x (~400.2 eV) in WN_xC_y. Finally, we could observe two distinct peaks in the C 1s spectra (Fig. 8c). While the C1s peak at 284.6 eV appeared from amorphous C, the peak at lower BE of ~ 280.5 eV could be assigned to the C in W-C_x. It is reported in the literature that the C 1s in WC_x lies within a BE of 279.7–283.8 eV [61]. On the other hand, the Cl 2p shows a prominent peak centered at ~ 199 eV corresponding to metal chloride (Cl $2p_{3/2}$ lies at ~ 198.7 eV) and hence. Therefore, it is concluded that TBH cannot grow W metal nor tungsten nitride. Instead, WCl_5 and TBH most possibly deposit WC_xN_y, as evident from the XRD and XPS analysis together. Though it was reported in the literature that TBH, as a reactant, could give rise to metal film as well as its nitride, the experimental findings for this case complement the DFT results of forming a ternary carbonitride compound to a good extent with significant impurities [23,62].

The high-resolution XP spectra of W 4f and N 1s electrons detected for the films deposited using WCl_5 and NH_3 ensure the formation of tungsten nitride films, as can be seen from Fig. 9. The BEs for W 4f electrons are also expected to lie at lower values of ~ 31.6 eV ($4f_{7/2}$) and at 33.7 eV ($4f_{5/2}$) that corresponds to $W^{+\delta}$ in W_2N [63,64]. In addition, the N 1s peak centered at ~ 396.8 eV is also a signature peak for W-N bonding which is well-matched with the existing literature [65]. The atomic% ratio of W/N as approximately 64.7:34.8 obtained from this XPS measurement also revealed the film to be most likely W_2N. However, unlike the ALD of metallic-W films deposited either with H_2 plasma or with DEAB, the XPS for W_2N films revealed a negligible and broad peak for Cl 2p at BE around 196.9 to 200.6 eV.

The films deposited with TEA as a reactant reveal the XPS peaks for WC_x as confirmed from the W 4f (at 32.1 and 34.1 eV for $4f_{7/2}$ and $4f_{5/2}$, respectively) and C1s (at 283.3 eV) peaks (Fig. S4), complementing the theoretical prediction via DFT calculations. However, the W 4f spectra also show prominent peaks corresponding to the formation of WO_3 at BE of above 36 eV. Therefore, these films contain a significant amount of oxides owing to the possible formation of WO_xC_y. In addition, we also find significant XPS peaks for both Cl 2p and Al 2p in the XPS, reflecting a considerable incomplete reaction between WCl_5 and TEA under this reaction condition. Though it is out of the scope of the current study, a higher deposition temperature might lead to the pure formation of WC_x, which may also inhibit the oxide formation in the films to some extent.

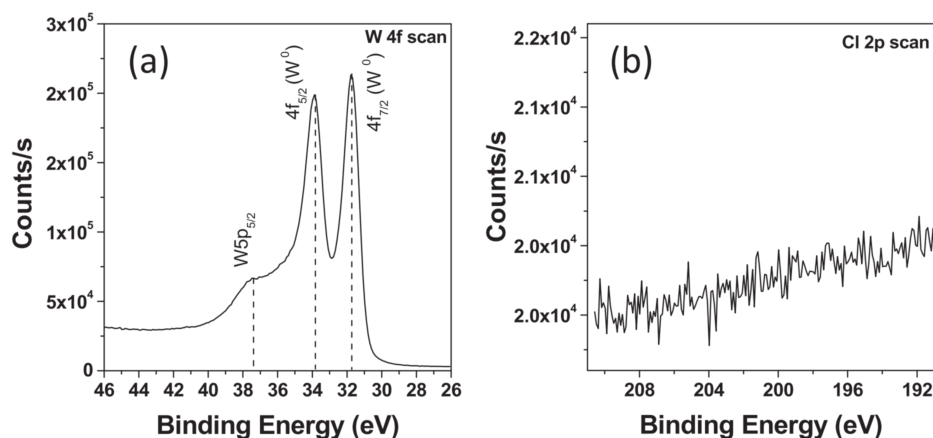

Fig. 7. XPS peaks for (a) W4f and (b) Cl2p orbital electrons for the films grown with WCl_5 and H_2 plasma reactant.

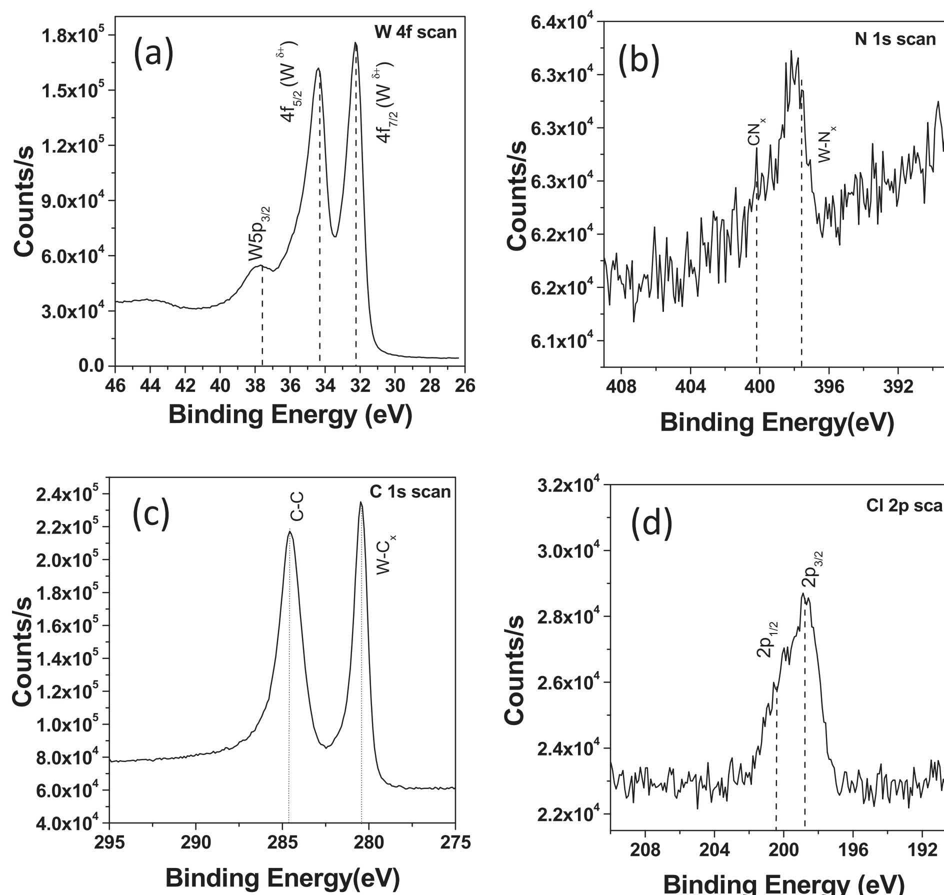

Fig. 8. XPS peaks for (a) W4f, (b) N1s, and (c) Cl2p orbital electrons for the films grown with WCl_5 and TBH.

Finally, Fig. S5 shows the individual XPS spectra of possible elements that could be present in the films deposited with DEAB as a reactant. While the W 4f peaks are similarly located at relatively higher BEs of ~ 32.1 and 34.3 eV for $4f_{7/2}$ and $4f_{5/2}$, respectively, not well-defined (or negligible) peaks are observed for both C 1s and N 1s. Therefore, unlike TBH and TEA, DEAB is neither expected to give rise to pure WN_xC_y nor WC_x, respectively. The presence of the B-N bond in the amine-borane complex is expected to hinder the incorporation of the nitrogen atom in the deposited film. As shown in DFT results (Fig. 2), the chemisorption of DEAB with W-N bond formation showed the endothermic process due to the reaction require the B-N bond dissociation for –W-N$(C_2H_5)_2$* formation of P(VI) and –W-N$(C_2H_5)_2$-BH_3* formation of P(VIII) exhibit a steric hindrance effect. Different from DEAB, an amine-based reactant such as NH_3 or TBH only would act as a nitriding agent. Therefore, we believe it to be an amorphous W film that consists of little amount of WN_xC_y formation along with significant O incorporation as revealed by the W 4f spectra itself. The high-resolution XPS for W 4f obtained with such four prominent peaks (two for WO_3) from metal W films is in well agreement with the previous literature [62]. On the other hand, considerable peaks for B 1s and Cl 2p are also observed. Interestingly, the Cl 2p peaks do not correspond to any metal–Cl bond, which indicates that DEAB may lead to a complete reaction compared to TEA against WCl_5. There might be some partial decomposition of DEAB at this deposition temperature leading to the presence of B in the film. In short,

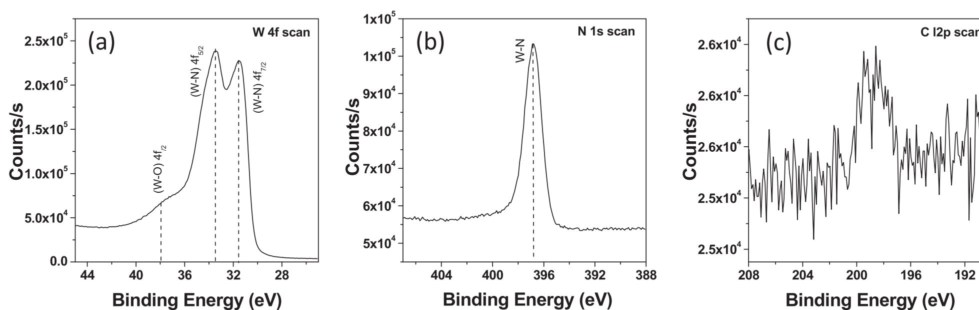

Fig. 9. XPS peaks for (a) W 4f, (b) N 1s, and (c) Cl 2p orbital electrons as grown W_2N thin films deposited via ALD using WCl_5 and NH_3.

the XPS analyses confirm the formation of β-W and amorphous W (with significant contamination) with H_2 plasma and DEAB, respectively. In addition, we can successfully deposit W_2N, WN_xC_y, and WC_x using NH_3, TBH, and TEA, respectively, as reactants. Therefore, the experimental evidence is in good agreement with the predictions of DFT calculations performed with all of those different reducing agents.

Table S2 gives a synopsis of the several essential parameters of the as-grown films deposited with different reactants. While crystalline films of β-W and c-W_2N were evident with H_2 plasma and NH_3, respectively, poor or nano-crystalline WN_xC_y films were formed with TBH. On the other hand, amorphous WC_x films with considerable O and Al should be expected with the reaction between WCl_5 and TMA. Similarly, amorphous W films with significant O incorporation along with some N and C were estimated with the DEAB as a reducing agent. It is expected that relatively porous and amorphous films were deposited by thermal ALD using TEA and DEAB, which might result in more oxygen incorporation in them. Here it is noteworthy to mention that the atomic percentage of Cl was truly negligible in the films deposited with H_2 plasma and NH_3. However, Cl was also not considerable impurity in the films deposited with other reactants. The density of ALD-W film deposited using H_2 plasma was as high as ~ 16.8 g cm^{-3}, which is close to its bulk value (~19.25 g-cm^{-3}). On the other hand, the as-deposited W_2N films revealed relatively lower mass density (~10.1 g-cm^{-3}) than that of its bulk value which could also be observed for several earlier reports on different ALD films. The W thin films deposited with H_2 plasma as a reducing agent shows considerably low resistivity of approximately 395 μΩ-cm, which is higher than the bulk resistivity of W-metal. However, the β-W is supposed to possess much higher resistivity (~100–300 μΩ-cm) compared to the most stable α-phase of the metal-W (5.6 μΩ-cm). Therefore, the relatively higher resistivity for the ALD-W obtained in the current study is in good agreement with the obtained crystalline phase in the present study. The resistivity could be reduced further upon post-annealing in an inert or reducing environment owing to its phase transformation (from β- to α-W) as well as by removing any negligible amount of surface and/or bulk contamination like O or Cl. Except for the films grown with H_2 plasma, all other films show significantly high resistivity primarily due to the impurities incorporated in them.

4. Conclusions

The article presents a comprehensive theoretical and experimental study to establish F-free W-precursor (WCl_5) toward ALD of W and other W-based films (W_2N, WC_x, and WN_xC_y). The rigorous DFT calculations recognize few suitable reactants among several possible reducing agents that can deposit W-metal from this FFW-precursor. DFT calculations show its ability to check the feasibility of the possible reaction pathways between reducing agent candidates and tungsten chlorides modeled by W_4Cl_{12} for ALD of W as well as to predict the composition of deposited films. In addition, the experiments validate the successful deposition of ALD-W in a temperature range of 200–300 °C using DEAB and H_2 plasma, all of which revealed exothermicity in DFT calculations. Mix-phase (predominantly β-phase) crystalline-W thin films with low resistivity are obtained using WCl_5 and H_2 plasma. A negligible percentage of Cl in the as-grown films indicates the complete reaction during ALD and thus the significance of the current process. However, a significantly high level of impurities was observed when DEAB was used as the reactant, leading to the amorphous nature of the film. In addition, nano-crystalline WN_xC_y films are evident with TBH, whereas amorphous WC_x films with significant O impurities were deposited at 300 °C when TEA was used as the reactant. Finally, the successful deposition of cubic-W_2N is also observed and investigated using WCl_5 and NH_3 molecules within the same temperature window and negligible Cl impurity. Thus, the current results not only help to select the reducing agents while exploring WCl_5 as a potential ALD precursor to deposit W thin films but also brings out the possibility of several other W-based films that could be prepared and studied to pave a future avenue.

Declaration of Competing Interest

The authors declare that they have no known competing financial interests or personal relationships that could have appeared to influence the work reported in this paper.

Acknowledgments

This work was financially supported by the MOTIE [Ministry of Trade, Industry & Energy (#10080651)] and KSRC (Korea Semiconductor Research Consortium) support program for the development of the future semiconductor device and the Advanced Technology Center Program (#10077265) funded by the MOTIE (Ministry of Trade, Industry & Energy) of the Republic of Korea. The precursor and reactants used in this study were provided by Hansol Chemical Co. Ltd. and Lake Materials Co. Ltd., Republic of Korea.

Appendix A. Supplementary material

Supplementary data to this article can be found online at https://doi.org/10.1016/j.apsusc.2021.150373.

References

[1] C.S. Hwang, Atomic Layer Deposition for Microelectronic Applications, in: N. Pinna, M. Knez (Eds.), Atomic Layer Deposition of Nanostructured Materials, Wiley-VCH Verlag GmbH & Co. KGaA, Weinheim, Germany, 2012, pp. 159–192, https://doi.org/10.1002/9783527639915.ch8.

[2] F. Lee, S. Marcus, E. Shero, G.W.J. Swerts, J.W. Maes, T. Blomberg, Atomic layer deposition: An enabling technology for microelectronic device manufacturing, in: 2007 IEEE/SEMI Advanced Semiconductor Manufacturing Conference, Stresa, Italy, 11–12 June 2007 (IEEE, Piscataway, New Jersey, 2000) pp. 359–365. https://doi.org/10.1109/ASMC.2007.375064.

[3] H. Kim, Atomic layer deposition of metal and nitride thin films: Current research efforts and applications for semiconductor device processing, J. Vac. Sci. Technol. B 21 (2003) 2231–2261, https://doi.org/10.1116/1.1622676.

[4] C. Zhao, J. Xiang, Atomic layer deposition (ALD) of metal gates for CMOS, Appl. Sci. 9 (2019) 2388, https://doi.org/10.3390/app9112388.

[5] B. Kalanyan, M.D. Losego, C.J. Oldham, G.N. Parsons, Low-temperature atomic layer deposition of tungsten using tungsten hexafluoride and highly-diluted silane

in argon, Chem. Vap. Deposition 19 (2013) 161–166, https://doi.org/10.1002/cvde.201307053.

[6] G. Wang, Q. Xu, T. Yang, J. Xiang, J. Xu, J. Gao, C. Li, J. Li, J. Yan, D. Chen, T. Ye, C. Zhao, J. Luoz, Application of atomic layer deposition tungsten (ALD W) as gate filling metal for 22 nm and beyond nodes CMOS technology, ECS J. Solid State Sci. Technol. 3 (2014) P82–P85, https://doi.org/10.1149/05810.0317ecst.

[7] J.W. Klaus, S.J. Ferro, S.M. George, Atomic layer deposition of tungsten using sequential surface chemistry with a sacrificial stripping reaction, Thin Solid Films 360 (2000) 145–153, https://doi.org/10.1016/S0040-6090(99)01076-7.

[8] J.W. Elam, J.A. Libera, M.J. Pellin, A.V. Zinovev, J.P. Greene, J.A. Nolen, Atomic layer deposition of W on nanoporous carbon aerogels, Appl. Phys. Lett. 89 (2006), 053124, https://doi.org/10.1063/1.2245216.

[9] S.-H. Kim, N. Kwak, J. Kim, H. Sohn, A comparative study of the atomic-layer-deposited tungsten thin film as nucleation for W-plug deposition, J. Electrochem. Soc. 153 (2006) G887–G893, https://doi.org/10.1149/1.2222966.

[10] D. Choi, K. Barmak, On the potential of tungsten as next-generation semiconductor interconnects, Electron. Mater. Lett. 13 (2017) 449–456, https://doi.org/10.1007/s13391-017-1610-5.

[11] C.-H. Kim, I.-C. Rho, S.-H. Kim, I.-K. Han, H.-S. Kang, S.-W. Ryu, H.-J. Kim, Pulsed CVD-W nucleation layer using WF_6 and B_2H_6 for low resistivity W, J. Electrochem. Soc. 156 (2009) H685–H689, https://doi.org/10.1149/1.3155430.

[12] P. Rodriguez, R. Famulok, Y.L. Friec, J.-P. Reynard, B.-N. Bozon, F. Boyer, K. Dabertrand, C. Jahana, S. Favier, Y. Mazel, B. Previtali, P. Gergaud, F. Nemouchi, Advanced characterizations of fluorine-free tungsten film and its application as low resistance liner for PCRAM, Mater. Sci. Semicond. Process. 71 (2017) 433–440, https://doi.org/10.1016/j.mssp.2017.08.033.

[13] K.J. Blakeney, C.H. Winter, Thermal atomic layer deposition of tungsten carbide films from WCl_6 and $AlMe_3$, J. Vac. Sci. Technol. A 36 (2018) 01A104, https://doi.org/10.1116/1.5002667.

[14] J.S. Becker, S. Suh, S. Wang, R.G. Gordon, Highly conformal thin films of tungsten nitride prepared by atomic layer deposition from a novel precursor, Chem. Mater. 15 (2003) 2969–2976, https://doi.org/10.1021/cm021772s.

[15] C.L. Dezelah IV, O.M. El-Kadri, K. Kukli, K. Arstila, R.J. Baird, J. Lu, L. Niinisto, C. H. Winter, A low valent metalorganic precursor for the growth of tungsten nitride thin films by atomic layer deposition, J. Mater. Chem. 17 (2007) 1109–1116, https://doi.org/10.1039/B610873C.

[16] D.K. Nandi, U.K. Sen, S. Sinha, A. Dhara, S. Mitra, S.K. Sarkar, Atomic layer deposited tungsten nitride thin films as a new lithium-ion battery anode, Phys. Chem. Chem. Phys. 17 (2015) 17445–17453, https://doi.org/10.1039/C5CP02184G.

[17] T.E. Hong, J.-H. Jung, S. Yeo, T. Cheon, S.I. Bae, S.-H. Kim, S.J. Yeo, H.-S. Kim, T.-M. Chung, B.K. Park, C.G. Kim, Highly conformal amorphous W−Si−N thin films by plasma-enhanced atomic layer deposition as a diffusion barrier for Cu metallization, J. Phys. Chem. C 119 (2015) 1548–1556, https://doi.org/10.1021/jp510226g.

[18] J.B. Kim, B. Jang, H.-J. Lee, W.S. Han, D.-J. Lee, H.-B.-R. Lee, T.E. Hong, S.-H. Kim, A controlled growth of WN_x and WC_x thin films prepared by atomic layer deposition, Mater. Lett. 168 (2016) 218–222, https://doi.org/10.1016/j.matlet.2016.01.071.

[19] J.B. Kim, D.K. Nandi, T.H. Kim, Y. Jang, J.-S. Bae, T.E. Hong, S.-H. Kim, Atomic layer deposition of WN_x thin films using a F-free tungsten metal-organic precursor and NH_3 plasma as a Cu-diffusion barrier, Thin Solid Films 685 (2019) 398–401, https://doi.org/10.1016/j.tsf.2019.06.051.

[20] D.J. Hagen, I.M. Povey, S. Rushworth, J.S. Wrench, L. Keeney, M. Schmidt, N. Petkov, S.T. Barry, J.P. Coyle, M.E. Pemble, Atomic layer deposition of Cu with a carbene-stabilized Cu(I) silylamide, J. Mater. Chem. C 2 (2014) 9205–9214, https://doi.org/10.1039/C4TC01418A.

[21] L. Wu, E. Eisenbraun, Integration of atomic layer deposition-grown copper seed layers for Cu electroplating applications, J. Electrochem. Soc. 156 (2009) H734–H739, https://doi.org/10.1149/1.3166184.

[22] B. Vidjayacoumar, D.J.H. Emslie, J.M. Blackwell, S.B. Clendenning, J.F. Britten, Solution reactions of a bis(pyrrolylaldiminate)copper(II) complex with peralkyl zinc, aluminum, and boron reagents: Investigation of the pathways responsible for copper metal deposition, Chem. Mater. 22 (2010) 4854–4866, https://doi.org/10.1021/cm101443x.

[23] K. Väyrynen, K. Mizohata, J. Räisänen, D. Peeters, A. Devi, M. Ritala, M. Leskalä, Low-temperature atomic layer deposition of low-resistivity copper thin films using $Cu(dmap)_2$ and tertiary butyl hydrazine, Chem. Mater. 29 (2017) 6502–6510, https://doi.org/10.1021/acs.chemmater.7b02098.

[24] B.S. Lim, A. Rahtu, R.G. Gordon, Atomic layer deposition of transition metals, Nat. Mater. 2 (2003) 749–754, https://doi.org/10.1038/nmat1000.

[25] K.J. Blakeney, C.H. Winter, Atomic layer deposition of aluminum metal films using a thermally stable aluminum hydride reducing agent, Chem. Mater. 30 (2018) 1844–1848, https://doi.org/10.1021/acs.chemmater.8b00445.

[26] G. Dey, S.D. Elliot, Quantum chemical study of the effect of precursor stereochemistry on dissociative chemisorption and surface redox reactions during the atomic layer deposition of the transition metal copper, J. Phys. Chem. C. 119 (2015) 5914–5927, https://doi.org/10.1021/jp509334u.

[27] J.P. Coyle, G. Dey, E.R. Sirianni, M.L. Kemell, G.P.A. Yap, M. Ritala, S.D. Elliot, S. T. Barry, Deposition of copper by plasma-enhanced atomic layer deposition using a novel N-heterocyclic carbene precursor, Chem. Mater. 25 (2013) 1132–1138, https://doi.org/10.1021/cm400215q.

[28] G. Dey, S.D. Elliot, Copper reduction and atomic layer deposition by oxidative decomposition of formate by hydrazine, RSC Adv. 4 (2014) 34448–34453, https://doi.org/10.1039/C4RA07003H.

[29] R. Hidayat, T. Chowdhury, Y. Kim, S. Kim, T.R. Mayangsari, S.-H. Kim, W.-J. Lee, Density functional theory study on the reducing agents for atomic layer deposition of tungsten using tungsten chloride precursor, Appl. Surf. Sci. 538 (2021), 148156, https://doi.org/10.1016/j.apsusc.2020.148156.

[30] S.D. Elliott, G. Dey, Y. Maimaiti, Classification of processes for the atomic layer deposition of metals based on mechanistic information from density functional theory calculations, J. Chem. Phys. 146 (2017), 052822, https://doi.org/10.1063/1.4975085.

[31] B. Delley, From molecules to solids with the $DMol^3$ approach, J. Chem. Phys. 113 (2000) 7756–7764, https://doi.org/10.1063/1.1316015.

[32] J.P. Perdew, K. Burke, M. Ernzerhof, Generalized gradient approximation made simple, Phys. Rev. Lett. 77 (1996) 3865–3868, https://doi.org/10.1103/PhysRevLett.77.3865.

[33] B. Delley, An all-electron numerical method for solving the local density functional for polyatomic molecules, J. Chem. Phys. 92 (1990) 508–517, https://doi.org/10.1063/1.458452.

[34] A. Bergner, M. Dolg, W. Küchle, H. Stoll, H. Preuß, Ab initio energy-adjusted pseudopotentials for elements of groups 13–17, Mol. Phys. 80 (1993) 1431–1441, https://doi.org/10.1080/00268979300103121.

[35] M. Dolg, U. Wedig, H. Stoll, H. Preuss, Energy-adjusted ab initio pseudopotentials for the first row transition elements, J. Chem. Phys. 86 (1987) 866–872, https://doi.org/10.1063/1.452288.

[36] U.V. Barth, L. Hedin, A local exchange-correlation potential for the spin polarized case: I, J. Phys. C Solid State Phys. 5 (1972) 1629–1642, https://doi.org/10.1088/0022-3719/5/13/012.

[37] L.L. Yusup, J.-M. Park, Y.-H. Noh, S.-J. Kim, W.-J. Lee, S. Park, Y.-K. Kwon, Reactivity of different surface sites with silicon chlorides during atomic layer deposition of silicon nitride, RSC Adv. 6 (2016) 68515–68524, https://doi.org/10.1039/C6RA10909H.

[38] T.R. Mayangsari, L.L. Yusup, J.-M. Park, E. Blanquet, M. Pons, J. Jung, W.-J. Lee, Study of surface reaction during selective epitaxy growth of silicon by thermodynamic analysis and density functional theory calculation, J. Cryst. Growth. 468 (2017) 278–282, https://doi.org/10.1016/j.jcrysgro.2017.01.006.

[39] L.L. Yusup, J.-M. Park, T.R. Mayangsari, Y.-K. Kwon, W.J. Lee, Surface reaction of silicon chlorides during atomic layer deposition of silicon nitride, Appl. Surf. Sci. 432 (2018) 127–131, https://doi.org/10.1016/j.apsusc.2017.06.060.

[40] A.A. Zinn, Chemical Vapor Deposition of Tungsten, in: T.T. Kodas, M.J. Hampden-Smith (Eds.), The Chemistry of Metal CVD, Wiley-VCH Verlag GmbH & Co. KGaA, Weinheim, Germany, 1994, pp. 105–174, https://doi.org/10.1002/9783527615858.ch3.

[41] S.-H. Kim, N. Kwak, J. Kim, H. Sohn, A comparative study of the atomic-layer-deposited tungsten thin films as nucleation layers for W-Plug deposition, J. Electrochem. Soc. 153 (2006) G887–G893, https://doi.org/10.1149/1.2222966.

[42] C.A.V.D. Jeugd, G.J. Leusink, G.C.A.M. Janssen, S. Radelaar, Selective chemical vapor deposition of tungsten using WF_6 and GeH_4, Appl. Phys. Lett. 57 (1990) 354–356, https://doi.org/10.1063/1.103690.

[43] R. Humayun, S. Manandhar, M. Danek, Tungsten deposition process using germanium-containing reducing agent, US Pat. 9,159,571 B2, 2015.

[44] J.-M. Park, K. Jin, B. Han, M.J. Kim, J. Jung, J.J. Kim, W.-J. Lee, Atomic layer deposition of copper nitride film and its application to copper seed layer for electrodeposition, Thin Solid Films 556 (2014) 434–439, https://doi.org/10.1016/j.tsf.2014.01.034.

[45] T.J. Knisley, T.C. Ariyasena, T. Sajavaara, M.J. Saly, C.H. Winter, Low temperature growth of high purity, low resistivity copper films by atomic layer deposition, Chem. Mater. 23 (2011) 4417–4419, https://doi.org/10.1021/cm202475e.

[46] B. Vidjayacoumar, D.J.H. Emslie, S.B. Clendenning, J.M. Blackwell, J.F. Britten, A. Rheingold, Investigation of $AlMe_3$, BEt_3, and $ZnEt_2$ as co-reagents for low-temperature copper metal ALD/Pulsed-CVD, Chem. Mater. 22 (2010) 4844–4853, https://doi.org/10.1021/cm101442e.

[47] L.C. Kalutarage, S.B. Clendenning, C.H. Winter, Low-temperature atomic layer deposition of copper films using borane dimethylamine as the reducing co-reagent, Chem. Mater. 26 (2014) 3731–3738, https://doi.org/10.1021/cm501109r.

[48] N. Govind, M. Petersen, G. Fitzgerald, D. King-Smith, J. Andzelm, A generalized synchronous transit method for transition state location, Comput. Mater. Sci. 28 (2003) 250–258, https://doi.org/10.1016/S0927-0256(03)00111-3.

[49] T. Weckman, K. Laasonen, First principles study of the atomic layer deposition of alumina by TMA–H_2O-process, Phys. Chem. Chem. Phys. 17 (2015) 17322–17334, https://doi.org/10.1039/C5CP01912E.

[50] M. Shirazi, S.D. Elliott, Cooperation between adsorbates accounts for the activation of atomic layer deposition reactions, Nanoscale. 7 (2015) 6311–6318, https://doi.org/10.1039/c5nr00900f.

[51] J.W. Klaus, S.J. Ferro, S.M. George, Atomic layer deposition of tungsten nitride films using sequential surface reactions, J. Electrochem. Soc. 147 (2000) 1175–1181, https://doi.org/10.1149/1.1393332.

[52] K.-E. Elers, V. Saanila, W.-M. Li, P.J. Soininen, J.T. Kostamo, S. Haukka, J. Juhanoja, W.F.A. Besling, Atomic layer deposition of W_xN/TiN and WN_xC_y/TiN nanolaminates, Thin Solid Films 434 (2003) 94–99, https://doi.org/10.1016/S0040-6090(03)00501-7.

[53] S.-H. Kim, S.S. Oh, H.-M. Kim, D.-H. Kang, K.-B. Kim, W.-M. Li, S. Haukka, M. Tuominen, Characterization of atomic layer deposited WN_xC_y thin film as a diffusion barrier for copper metallization, J. Electrochem. Soc. 151 (2004) C272–C282, https://doi.org/10.1149/1.1652054.

[54] M.J. O'Keefe, J.T. Grant, J.S. Solomon, Magnetron sputter deposition of A-15 and BCC crystal structure tungsten thin films, J. Electron. Mater. 24 (1995) 961–967, https://doi.org/10.1007/BF02652968.

[55] F. Zhu, Z. Xie, Z. Zhang, Phase control and Young's modulus of tungsten thin film prepared by dual ion beam sputtering deposition, AIP Adv. 8 (2018), 035321, https://doi.org/10.1063/1.5021009.

[56] J.-S. Lee, J. Cho, C.-Y. You, Growth and characterization of α and β-phase tungsten films on various substrates, J. Vac. Sci. Technol. A 34 (2016), 021502, https://doi.org/10.1116/1.4936261.

[57] Q. Hao, W. Chen, G. Xiao, Beta (β) tungsten thin films: Structure, electron transport, and giant spin Hall effect, Appl. Phys. Lett. 106 (2015), 182403, https://doi.org/10.1063/1.4919867.

[58] C.T. O'Donohue, K.R. McClain, A. Koley, J.C. Revelli, L. McElwee-White, T. J. Anderson, Low temperature deposition of WN_xC_y diffusion barriers using WN $(NEt_2)_3$ as a single-source precursor, ECS J. Solid State Sci. Technol. 4 (2015) N3180–N3187, https://doi.org/10.1149/2.0251501jss.

[59] S.-H. Kim, J.-K. Kim, J.H. Lee, N. Kwak, J. Kim, S.-H. Jung, M.-R. Hong, S.H. Lee, J. Collins, H. Sohn, Characteristics of ALD tungsten nitride using B_2H_6, WF_6, and NH_3 and application to contact barrier layer for DRAM, J. Electrochem. Soc. 154 (2007) D435–D441, https://doi.org/10.1149/1.2742913.

[60] H.S. Sim, S.-I. Kim, Y.T. Kim, Method to enhance atomic-layer deposition of tungsten–nitride diffusion barrier for Cu interconnect, J. Vac. Sci. Technol. B 21 (2003) 1411–1414, https://doi.org/10.1116/1.1592806.

[61] D. Kim, O.H. Kim, T. Anderson, J. Koller, L. McElwee-White, L.-C. Leu, J.M. Tsai, D. P. Norton, Chemical vapor deposition of WN_xC_y using the tungsten piperidylhydrazido complex $Cl_4(CH_3CN)W(N\text{-}pip)$: Deposition, characterization, and diffusion barrier evaluation, J. Vac. Sci. Technol. A 27 (2009) 943–950, https://doi.org/10.1116/1.3106625.

[62] K. Väyrynen, T. Hatanpää, M. Mattinen, M.J. Heikkilä, K. Mizohata, J. Räisänen, J. Link, R. Stern, M. Ritala, M. Leskelä, Atomic layer deposition of nickel nitride thin films using $NiCl_2$(TMPDA) and tert-butylhydrazine as precursors, Phys. Status Solidi A 216 (2019) 1900058, https://doi.org/10.1002/pssa.201900058.

[63] P.-C. Jiang, Y.-S. Lai, J.S. Chen, Dependence of crystal structure and work function of WN_x films on the nitrogen content, Appl. Phys. Lett. 89 (2006), 122107, https://doi.org/10.1063/1.2349313.

[64] C. Metaxa, B.D. Ozsdolay, T. Zorba, K. Paraskevopoulos, D. Gall, P. Patsalas, Electronic and optical properties of rocksalt-phase tungsten nitride (B1-WN), J. Vac. Sci. Technol. A 35 (2017), 031501, https://doi.org/10.1116/1.4978030.

[65] C. Meunier, C. Monteil, C. Savall, F. Palmino, J. Weber, R. Berjoan, J. Durand, RBS-ERDA, XPS and XRD characterizations of PECVD tungsten nitride films, Appl. Surf. Sci. 125 (1998) 313–320, https://doi.org/10.1016/S0169-4332(97)00383-8.